www.editada.org

_____

Robust Linear Discrete Control for a Hexacopter: Experimental Results

Omar-Jacobo Santos-Sánchez[1], Mario Ordaz[2], Patricio Ordaz[1],
Hugo Romero-Trejo[1], Orlando García-Pérez[1]

[1]Research Center on Technology of Information and Systems, Autonomous University of Hidalgo State, Pachuca, Hidalgo, México

[2]Departamento de Ingeniería Eléctrica y Electrónica, TecNM / Campus Pachuca (IT Pachuca)

E-mails: omarj@uaeh.edu.mx
mario.oo@pachuca.tecnm.mx
jesus_ordaz@uaeh.edu.mx
rhugo@uaeh.edu.mx
orlando_garcia@uaeh.edu.mx

Abstract. This paper presents a discrete-time robust linear control method for tracking a hexacopter's trajectory in the presence of external disturbances. The control of multi-rotor type unmanned aerial vehicles (UAVs) has gained considerable attention recently due to their various applications, such as crop spraying in precision agriculture. The control of UAVs requires robustness to reject disturbances and accommodate dynamic uncertainties. To achieve this goal, the robust discrete-time control action is designed in two stages. The first stage utilizes the solution of a difference Riccati-equation to guarantee system stability in an optimal sense. The second stage provides system robustness against external disturbances and uncertain dynamics. Furthermore, the Lyapunov stability theory for discrete linear systems is used to derive system asymptotic stability. Finally, experimental results of the hexacopter flight are provided to illustrate the effectiveness of the presented control law.

Keywords: Hexacopter, stability, disturbances, discrete-time system, uncertainties, robust control.

1 Introduction

In recent years, unmanned aerial vehicles (UAVs) have become a subject of study for the control community due to their numerous applications. These include monitoring and inspecting areas with limited access, biodiversity conservation, aerial inspection and chemical spraying of crops, monitoring energy facilities and pipelines, and monitoring air quality, as noted by Tyokumbur, E. T. [25] and Sanca, A. S. [25]. However, the challenges that UAVs present for automatic control cannot be ignored. The different applications of automatic control in UAVs require analyzing the problems that may arise. According to Tripolitsiotis, A. [24], the main challenges facing the control design for UAVs are the autonomy of operating time and the robustness of the controller against external disturbances generated by wind currents. Multirotor type UAVs have captured attention as they offer significant advantages over other aircraft. An unmanned aerial vehicle with a greater number of motors can move larger loads, which means more power but also greater energy consumption, resulting in reduced autonomy time. According to Arellano-Muro, C. A. [4], the hexacopter configuration and its number of motors allow for better load distribution in its structure, as well as the transport of objects with greater mass compared to UAVs with smaller numbers of motors.

Generally, the dynamic model of UAVs is studied by obtaining the Euler-Lagrange equations. Subsequently, under certain assumptions, the principle of separation of dynamics into subsystems is used for control purposes. Various solutions have been proposed to solve some of the problems associated with the control of UAVs, particularly hexacopters. For example, Rajappa, S. [21] proposes a different architecture to the traditional one, where the propellers are inclined and controlled using linearizing feedback. Durham, W. C. [10] studies the problem of minimization by assigning several controls for the generation of specific moments of the body axis in the UAV. Alaimo, A. [3] employs a linear quadratic regulator to tune a PD controller and a PID for height control tasks, which reduces the steady-state error to zero and stabilizes the hexacopter. Pose, C. D. [20] proposes an optimal control that minimizes the force exerted by the motors, which improves the maneuverability of the system by

considering different actuators restrictions. Falconi, G. P. [11] presents an adaptive backstepping control that tolerates different disturbances and considers a linear model for the actuators. Busarakum, S. [8] designs a controller with sliding modes on the dynamic model of a hexacopter for altitude control tasks, which is insensitive to external disturbances and uncertainties in the parameters. Artale, V. [5] approximates the mathematical model and control for a UAV using a neural network suitable for stabilization and trajectory tracking tasks. Ao Bai [7] discusses trajectory tracking with yaw angle control for a quadrotor UAV that contemplates non-modeled parametric and dynamic disturbances. The control proposal presented in [7] involves a robust method based on L_2 gain and dissipation theory that demonstrates uniform ultimate error bounds. The authors decompose the dynamics of the UAV into subsystems to separately control position and height and provide simulation results to validate their approach. In contrast, Mohammad Javad Mahmoodabadi proposes a robust adaptive backstepping controller in [17] for stabilizing a UAV with highly nonlinear dynamics and strong coupling. By using the descending gradient method and sliding modes, the controller parameters are adjusted to improve the UAV's response to disturbances and uncertainties in the model. Later on, Ghulam E Mustafa Abro [1] presents a contribution where he uses an optimization algorithm to reduce both the error and energy consumption of a quadrotor UAV. He also presents the experimental results of his proposal. In his contribution, he designs an intelligent controller for trajectory following tasks. To obtain the nonlinear dynamics of the UAVs using the Newton Euler method, Abro proposes a state observer. This is necessary since the UAV is, by nature, an underactuated system. The proposed height control is designed using fuzzy-based sliding modes, while the position control is obtained using hyperbolic functions. The authors present the numerical validation of their proposal. In another contribution, Chengxing Lv [16] proposes an energy-based control for USVs using perturbation observers. This method optimizes the energy and improves the performance of USVs in trajectory-following tasks, even in the presence of unknown environmental perturbations. In the first contribution, an observer is designed to estimate disturbances, and the control based on the observed energy allows for exponential convergence of the error to zero. The author presents a comparative study of simulation results to validate their proposal. In another paper, Pengyuan Shao [23] applies a model based on the variation of linear parameters, along with a structural PID controller robustly penalized in its proportional part, for flapping wing UAVs. The proposal developed can capture the response of the original nonlinear model with lower error than the Jacobian method for linearization. The numerical results allow the author to establish conditions for the designed controller to maintain stable flights with satisfactory robustness and performance in practice. It is worth noting that the results reported in the literature by the authors only present simulation results using a continuous time-domain mathematical model. They do not consider the implementation of their control laws on a hexacopter. Furthermore, their primary motivation differs from providing robustness to the control system, which is an important objective in any task involving external environments that can be assigned to hexacopter-type UAVs.

The article presents an experimentally validated robust linear control of discrete nature for linear systems subject to external disturbances. The controller has two terms linked to state feedback, one arbitrarily chosen and the other providing robustness to the system against disturbances. This controller is implemented on a hexacopter-type UAV, whose dynamics are divided into subsystems, linearized, and discretized around a fixed point, while still maintaining a centralized control system. The penalty of the controller parameters for the robust term could be solved in different ways. The main contributions of this work can be summarized as follows:

- By employing exact linearization in the hexacopter dynamics, it is possible to implement a discrete robust linear controller in a centralized manner for each of the subsystems to control the position and altitude.
- The implemented control law employs a discrete LQR controller in the first term, which penalizes a performance index to ensure stability in the optimal sense. At the same time, the second term guarantees asymptotic stability by defining the matrix P, a parameter of the robust control term, which gives a solution to the discrete-time Lyapunov equation used in its synthesis.
- The implemented control law endows the hexacopter with robustness in both autonomous and non-autonomous flights, thereby enabling the operator to perform complex maneuvers manually, thanks to the contribution of orientation control.

The document is organized as follows: Section 1 introduces the topic covered in this work and outlines the related literature published previously. In Section 2, we apply the Newton-Euler method to derive the dynamic model of the hexacopter, which is divided into subsystems and discretized around a fixed point using the Euler derivative. This enables separate control over x, y, and z positions, as well as roll, pitch, and yaw angles. Section 3 reports the synthesis of the discrete robust linear control, considering external perturbations and uncertainties. Section 4 describes the experimental platform, while Section 5 presents the numerical and experimental results. Finally, Section 6 provides the conclusions.

2 Dynamic Model

The hexacopter depicted in Figure 1 is a multi-rotor aircraft system that consists of six rotors. Traditionally, the mathematical model consists of two parts. The first part is defined by *(x, y, z)* and denotes the translational part, while the second part is defined by the East-North-Up (ENU) coordinates. In this work, the mathematical model of the multi-rotor aerial vehicle considered is proposed by Alaimo, A. [2], Arellano-Muro [4], and Moussid [18], and is as follows:

$$\ddot{x} = \frac{u\left(\sin\theta\sin\psi + \cos\psi\sin\phi\cos\theta\right)}{m}$$

$$\ddot{y} = \frac{u\left(-\cos\psi\sin\theta + \sin\psi\sin\phi\cos\theta\right)}{m}$$

$$\ddot{z} = \frac{u\left(\cos\phi\cos\theta\right)}{m} - g \tag{1}$$

$$\ddot{\theta} = \dot{\phi}\dot{\psi}\frac{\left(I_y - I_z\right)}{I_x} - \frac{J_p}{I_x}\Omega + \frac{l}{I_x}\tau_\theta$$

$$\ddot{\phi} = \dot{\theta}\dot{\psi}\frac{\left(I_x - I_z\right)}{I_y} + \frac{J_p}{I_y}\Omega + \frac{l}{I_y}\tau_\phi$$

$$\ddot{\psi} = \dot{\phi}\dot{\theta}\frac{\left(I_y - I_x\right)}{I_z} + \frac{l}{I_z}\tau_\psi \tag{2}$$

where I_x, I_y, I_z representing the inertia of the body, J_p defines the rotor-propeller inertia, $m = 1.7118$ kg is the mass of unmanned aerial vehicle (UAV), $\Omega = \omega_4 + \omega_2 + \omega_5 - \omega_1 - \omega_6 - \omega_3$, with ω_i are the angular speeds of the motors i, and τ_ϕ, τ_θ, τ_ψ are the torques that allow performing the swing-lift-turn movements defined below

$$\tau_\phi = l\left(f_1 + f_5 - f_6 - f_2\right)\cos 30°$$
$$\tau_\theta = l\left(f_3 - f_4 + \sin 30°\left(f_5 - f_1 + f_2 - f_6\right)\right) \tag{3}$$
$$\tau_\psi = c\left(f_1 + f_6 + f_3 - f_4 - f_2 - f_5\right),$$

where f_i is described as $f_i = k_i\omega_i^2$, $k_i = 1$ are positive constants, which refers to the scaling between the angular speed of the motor and the linear force produced, associated in this case with the thrust, $c = 0.5$ N is a constant parameter which refers to the scaling factor of force against moment, in this case it is related to the drag, and $l = 267.5$ mm is the center of mass length for each motor.
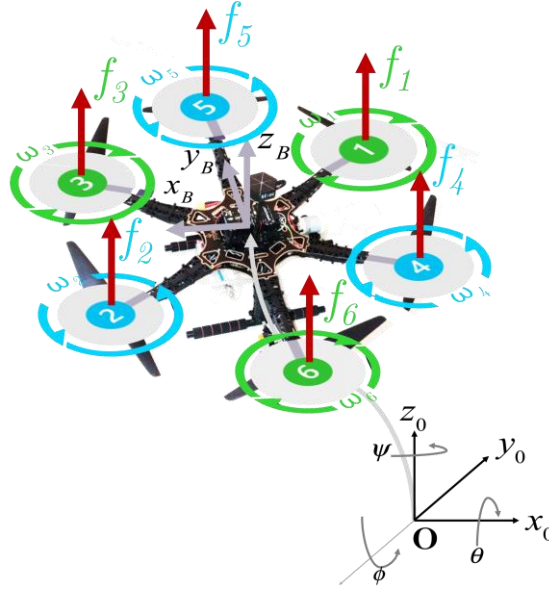
Figure 1. Coordenate frames in hexacopter.

To write, system (1)-(2) in the standard nonlinear system representation, consider next variable change $x_1 = x$, $x_2 = \dot{x}$, $x_3 = y$, $x_4 = \dot{y}$, $x_5 = z$, $x_6 = \dot{z}$, $x_7 = \theta$, $x_8 = \dot{\theta}$, $x_9 = \phi$, $x_{10} = \dot{\phi}$, $x_{11} = \psi$, $x_{12} = \dot{\psi}$, the inputs $u_1 = u$, $u_2 = \tau_\theta$, $u_3 = \tau_\phi$, $u_4 = \tau_\psi$, $u_5 = \Omega$. In this way and with the equations that describe the translational dynamics of the hexacopter defined by the equation (1) it is noted that the equation (2) can be expressed as follows:

$$\dot{x}_1 = x_2$$

$$\dot{x}_2 = \frac{u_1\left(\sin\left(x_7\right)\sin\left(x_{11}\right) + \cos\left(x_{11}\right)\sin\left(x_9\right)\cos\left(x_7\right)\right)}{m}$$

$$\dot{x}_3 = x_4$$

$$\dot{x}_4 = \frac{u_1\left(-\cos\left(x_{11}\right)\sin\left(x_7\right) + \sin\left(x_{11}\right)\sin\left(x_9\right)\cos\left(x_7\right)\right)}{m}$$

$$\dot{x}_5 = x_6$$

$$\dot{x}_6 = \frac{u_1\left(\cos\left(x_9\right)\cos\left(x_7\right)\right)}{m} - g \qquad (4)$$

$$\dot{x}_7 = x_8$$

$$\dot{x}_8 = x_{10}x_{12}\frac{\left(I_y - I_z\right)}{I_x} - \frac{J_p}{I_x}u_5 + \frac{l}{I_x}u_2$$

$$\dot{x}_9 = x_{10}$$

$$\dot{x}_{10} = x_8 x_{12}\frac{\left(I_x - I_z\right)}{I_y} + \frac{J_p}{I_y}u_5 + \frac{l}{I_y}u_3$$

$$\dot{x}_{11} = x_{12}$$

$$\dot{x}_{12} = x_{10}x_8 \frac{\left(I_y - I_x\right)}{I_z} + \frac{l}{I_z}u_4$$

Notice that, the above dynamical model can be written in subsystems z, ψ, $x-\phi$ and $y-\theta$. Therefore, these subsystems remain as:

$$z = \begin{cases} \dot{x}_5 = x_6 \\ \dot{x}_6 = \frac{u_1\left(\cos\left(x_9\right)\cos\left(x_7\right)\right)}{m} - g \end{cases}$$

$$\psi = \begin{cases} \dot{x}_{11} = x_{12} \\ \dot{x}_{12} = x_{10}x_8 \frac{\left(I_y - I_x\right)}{I_z} + \frac{l}{I_z}u_4 \end{cases}$$

$$x-\theta = \begin{cases} \dot{x}_1 = x_2 \\ \dot{x}_2 = \frac{u_1\left(\sin\left(x_7\right)\sin\left(x_{11}\right)+\cos\left(x_{11}\right)\sin\left(x_9\right)\cos\left(x_7\right)\right)}{m} \\ \dot{x}_7 = x_8 \\ \dot{x}_8 = x_{10}x_{12}\frac{\left(I_y - I_z\right)}{I_x} - \frac{J_p}{I_x}x_8u_5 + \frac{l}{I_x}u_2 \end{cases} \quad (5)$$

$$y-\phi = \begin{cases} \dot{x}_3 = x_4 \\ \dot{x}_4 = \frac{u_1\left(-\cos\left(x_{11}\right)\sin\left(x_7\right)+\sin\left(x_{11}\right)\sin\left(x_9\right)\cos\left(x_7\right)\right)}{m} \\ \dot{x}_9 = x_{10} \\ \dot{x}_{10} = x_8x_{12}\frac{\left(I_x - I_z\right)}{I_y} + \frac{J_p}{I_y}x_{10}u_5 + \frac{l}{I_y}u_3 \end{cases}$$

Proposing the controls $u_2^{'}$, $u_3^{'}$, $u_4^{'}$ and u_5 as:

$$u_2^{'} = -\frac{I_x}{l}\left(x_{10}x_{12}\frac{\left(I_y - I_z\right)}{I_x} - \frac{1}{I_x} - u_2 \right)$$

$$u_3^{'} = -\frac{I_y}{l}\left(x_8x_{12}\frac{\left(I_x - I_z\right)}{I_y} + \frac{1}{I_y} - u_3 \right) \quad (6)$$

$$u_4' = -\frac{I_z}{l}\left(x_{10}x_8\frac{(I_y - I_x)}{I_z} - u_4\right)$$

$$u_5 = \frac{1}{J_p}$$

On the other hand, the u_1 control is proposed as follows:

$$u_1 = \frac{m}{\cos(x_9)\cos(x_7)}(v+g)$$

(7)

and substituting this expression in the equation (5), an exact system linearization is achieved by means of states feedback, obtaining the following form for each subsystem:

$$z = \begin{cases} \dot{x}_5 = x_6 \\ \dot{x}_6 = v \end{cases}$$

$$\psi = \begin{cases} \dot{x}_{11} = x_{12} \\ \dot{x}_{12} = u_4 \end{cases}$$

$$x - \theta = \begin{cases} \dot{x}_1 = x_2 \\ \dot{x}_2 = \left(\tan(x_7)\frac{\sin(x_{11})}{\cos(x_9)} + \cos(x_{11})\tan(x_9)\right)(v+g) \\ \dot{x}_7 = x_8 \\ \dot{x}_8 = u_2 \end{cases}$$

(8)

$$y - \phi = \begin{cases} \dot{x}_3 = x_4 \\ \dot{x}_4 = \left(-\frac{\cos(x_{11})}{\cos(x_9)}\tan(x_7) + \sin(x_{11})\tan(x_9)\right)(v+g) \\ \dot{x}_9 = x_{10} \\ \dot{x}_{10} = u_3 \end{cases}$$

Next, by using Euler's method

$$x_{i+1}(k) = \frac{x_i(k+1) - x_i(k)}{h}$$

(9)

to obtain the discrete-time dynamics of subsystems described in (8). Thus, following discrete-time subsystems are attached. Subsystems z and ψ are given by:

$$z(k) = \begin{cases} x_5(k+1) = hx_6(k) + x_5(k) \\ x_6(k+1) = hv(k) + x_6(k) \end{cases}$$

$$\psi(k) = \begin{cases} x_{11}(k+1) = hx_{12}(k) + x_{11}(k) \\ x_{12}(k+1) = hu_4'(k) + x_{12}(k) \end{cases} \tag{10}$$

subsystem $x(k) - \theta(k)$ discreetly is written as:

$$x_1(k+1) = hx_2(k) + x_1(k)$$

$$x_2(k+1) = h\left(\tan(x_7(k))\frac{\sin(x_{11}(k))}{\cos(x_9(k))} + \cos(x_{11}(k))\tan(x_9(k))\right)(v(k) + g) + x_2(k)$$

$$x_7(k+1) = hx_8(k) + x_7(k)$$

$$x_8(k+1) = hu_2(k) + x_8(k)$$

subsystem $y(k) - \phi(k)$ discreetly is written as:

$$x_3(k+1) = hx_4(k) + x_3(k)$$

$$x_4(k+1) = h\left(-\frac{\cos(x_{11}(k))}{\cos(x_9(k))}\tan(x_7(k)) + \sin(x_{11}(k))\tan(x_9(k))\right)(v(k) + g) + x_4(k)$$

$$x_9(k+1) = hx_{10}(k) + x_9(k)$$

$$x_{10}(k+1) = hu_3(k) + x_{10}(k)$$

Just notice that previous subsystems representation can be represented in the standard linear discrete-time representation, in the way García, O., Santos, O. [12] uses it:

$$x(k+h) = Ax(k) + Bu(k) \tag{11}$$

Where the subsystem $z(k)$ is rewritten as:

$$\begin{bmatrix} x_5(k+1) \\ x_6(k+1) \end{bmatrix} = \begin{bmatrix} 1 & h \\ 0 & 1 \end{bmatrix} \begin{bmatrix} x_5(k) \\ x_6(k) \end{bmatrix} + \begin{bmatrix} 0 \\ h \end{bmatrix} v(k) \tag{12}$$

and the subsystem $\psi(k)$ in the form (11) is rewritten as:

$$\begin{bmatrix} x_{11}(k+1) \\ x_{12}(k+1) \end{bmatrix} = \begin{bmatrix} 1 & h \\ 0 & 1 \end{bmatrix} \begin{bmatrix} x_{11}(k) \\ x_{12}(k) \end{bmatrix} + \begin{bmatrix} 0 \\ h \end{bmatrix} u_4(k) \tag{13}$$

in the subsystems $x(k) - \theta(k)$ and $y(k) - \phi(k)$ some nonlinearities are evident. Due to this and the characteristics of the control to be implemented, a linearization of these subsystems is performed around the stable equilibrium, that is, at the origin. For example, in the subsystem $x(k) - \theta(k)$, the variable

$$x_1(k+1) = hx_2(k) + x_1(k)$$

linearized at the origin, it remains as:

$$x_1(k+1) = x_1(k)$$

Thus, the representation in state space of the discrete-time subsystem $x(k) - \theta(k)$, linearized at the origin is:

$$
\begin{bmatrix} x_1(k+1) \\ x_2(k+1) \\ x_7(k+1) \\ x_8(k+1) \end{bmatrix} = \begin{bmatrix} 1 & h & 0 & 0 \\ 0 & 1 & hg & 0 \\ 0 & 0 & 1 & h \\ 0 & 0 & 0 & 1 \end{bmatrix} \begin{bmatrix} x_1(k) \\ x_2(k) \\ x_7(k) \\ x_8(k) \end{bmatrix} + \begin{bmatrix} 0 \\ 0 \\ 0 \\ h \end{bmatrix} u_2(k)
$$

(14)

and the corresponding linearization for the subsystem $y(k) - \phi(k)$ is:

$$
\begin{bmatrix} x_3(k+1) \\ x_4(k+1) \\ x_9(k+1) \\ x_{10}(k+1) \end{bmatrix} = \begin{bmatrix} 1 & h & 0 & 0 \\ 0 & 1 & h & 0 \\ 0 & 0 & 1 & -hg \\ 0 & 0 & 0 & 1 \end{bmatrix} \begin{bmatrix} x_3(k) \\ x_4(k) \\ x_9(k) \\ x_{10}(k) \end{bmatrix} + \begin{bmatrix} 0 \\ 0 \\ 0 \\ h \end{bmatrix} u_3(k)
$$

(15)

On the other hand, the non-linear form of the subsystem $x(k) - \theta(k)$ can be rewritten as:

$$
\bar{x}(k+1) = f_0(\bar{x}(k)) + f_1(\bar{x}(k))\bar{u}(k)
$$

Where

$$
\bar{x}(k) = \begin{bmatrix} x_1(k) \\ x_2(k) \\ x_7(k) \\ x_8(k) \end{bmatrix}, \quad f_1(\bar{x}(k)) = \begin{bmatrix} 0 & 0 \\ -h\dfrac{\tan(x_9(k))}{\cos(x_7(k))} & 0 \\ 0 & 0 \\ 0 & h \end{bmatrix},
$$

$$
\bar{u}(k) = \begin{bmatrix} v(k) \\ u_3(k) \end{bmatrix}
$$

$$
f_0(\bar{x}(k)) = \begin{bmatrix} x_1(k) + hx_2(k) \\ x_2(k) - hg\dfrac{\tan(x_9(k))}{\cos(x_7(k))} \\ x_7(k) + hx_8(k) \\ x_8(k) \end{bmatrix}
$$

Where $k = 0, 1, \ldots, N$, with sampling time h.

The controller presented in this document is based on the main idea that the subsystems are linear (using exact linearization or assumptions about the orientation angles), and then the control capacity is verified in the local sense. Theoretically, the synthesized controllers could be applied without restrictions on the initial conditions and stable points. However, in practice, this is not always possible due to the assumption that the models are linear. To validate this, an experimental study is conducted.

3   Linear Robust Control Design

It is important to mention that the design of the control law presented here is based directly on Chen, Y. H. [9], and is applied to the linearized dynamics of a hexacopter. To the best of the authors' knowledge, this control law has been reported in the literature but has never been experimentally tested before.

To this end, consider the discrete-time difference equation (11), with disturbances as:

$$x(k+1) = Ax(k) + Bu(k) + Cv(x(k), \sigma(k), k),\qquad(16)$$

with $x(k_0) = x_0$, where $k \in K := \{0,1,2,\ldots\}$, the state $x(k) \in R^n$, the control $u(k) \in R^m$, the disturbance $v(\sigma(k)) \in R^p$ and the uncertainties $\sigma(k) \in R^s$. The matrices A, B and C are of appropriate dimensions. The value of mapping $\sigma(\cdot)$ is unknown. Hereafter, for the system (16), next assumptions are fulfilled, see for example Chen, Y. H.[9]:

Assumption 1. The pair (A, B) is stabilizable. That is, there is a constant gain matrix $K \in R^{m \times n}$, such that all eigenvalues of $\bar{A} = A + BK$ are strictly within the unit circle.

Assumption 2. The matrix B is of full rank: $rank(B) = m$.

Assumption 3. The mapping $v(\cdot)$ is continuous.

Assumption 4. There is a prescribed compact set $\Sigma \in R^s$, such that $\sigma(k) \in \ \forall \ k$.

Assumption 5. There is a matrix D, such that:

$$C = BD_.$$

In addition, there is a constant $\gamma_1 > 0$, such that for all $x \in R^n$, $\sigma \in \Sigma$, $k \in K$, as mentioned by Khalil, H.K.[15]:

$$v(x, \sigma, k) \leq \gamma_1 x.\qquad(17)$$

The objective is to design a control law $u(k)$ that is linear at $x(k)$, such that the resulting solution of the closed-loop system is asymptotically stable.

The control design is only based on the possible level of uncertainty (in this case Σ). For the uncertain system (16), the following control scheme is proposed by Chen, Y. H. [9].

$$u(k) = Kx(k) - \gamma B^\top P \bar{A} x(k)\qquad(18)$$

where $P > 0$ is the only solution of the Lyapunov equation for discrete-time linear systems

$$A^\top PA - P + Q = 0\qquad(19)$$

Note. The control scheme (18) consists of two parts: $Kx(k)$ and $-\gamma B^{\mathsf{T}} P\bar{A}x(k)$. The first to stabilize the nominal system, that is $x(k+1) = Ax(k) + Bu(k)$, while the second part is destined to offset the effect due to uncertainties.

Theorem 1. Consider the uncertain discrete-time system (16). Assume that the above assumptions are fulfilled. The control scheme (18) makes the system asymptotically stable if $\gamma > 0$ and

$$2\gamma\lambda_{\min}(Q) > 2\gamma\lambda_{\max}(B^{\mathsf{T}}PB)\left[\gamma B^{\mathsf{T}}P\bar{A}x + \gamma_1 Dx\right]^2$$
$$+\gamma_1 x^2$$

Given the candidate Lyapunov function in the form:

$$V(x(k)) = x^{\mathsf{T}}(k)Px(x) \qquad (20)$$

with the system (16) and equation (20), it must be for each $\sigma(\cdot)$:

$$\Delta V(x(k)) = V(x(k+1)) - V(x(k))$$

$$= \begin{bmatrix} Ax(k) \\ +Bu(k) \\ +Cv(x(k),\sigma(k),k) \end{bmatrix}^{\mathsf{T}} P \begin{bmatrix} Ax(k) \\ +Bu(k) \\ +Cv(x(k),\sigma(k),k) \end{bmatrix}$$

$$-x^{\mathsf{T}}(k)Px(k)$$

that is $\Delta V(x(k))$ or ΔV is

$$\Delta V = [Ax + Bu + BDv]^{\mathsf{T}} P[Ax + Bu + BDv]$$
$$-x^{\mathsf{T}}Px,$$

$$\Delta V = \begin{bmatrix} Ax \\ +B(Kx - \gamma B^{\mathsf{T}}P\bar{A}x) + BDv \end{bmatrix}^{\mathsf{T}} P \begin{bmatrix} Ax \\ +B(Kx - \gamma B^{\mathsf{T}}P\bar{A}x) + BDv \end{bmatrix}$$

$$-x^{\mathsf{T}}Px.$$

Considering for the nominal system $x(k+1) = Ax(k) + Bu(k)$, ΔV has the form:

$$\Delta V = [Ax + Bu]^{\mathsf{T}} P[Ax + Bu] - x^{\mathsf{T}}Px$$

and $u = Kx$, in this way, thereby, so:

$$\Delta V = [Ax + BKx]^{\mathsf{T}} P[Ax + BKx] - x^{\mathsf{T}}Px,$$
$$\Delta V = x^{\mathsf{T}}\bar{A}^{\mathsf{T}}P\bar{A}x - x^{\mathsf{T}}Px$$
$$\Delta V = x^{\mathsf{T}}\left[\bar{A}^{\mathsf{T}}P\bar{A} - P\right]x,$$

that satisfies the equation (19), therefore:

$$\Delta V = -x^\mathsf{T} Q x,$$

for the nominal system.

Therefore ΔV for the disturbed system (16) can be written as:

$$
\begin{aligned}
\Delta V &= -x^\mathsf{T} Q x \\
&+ \left[B\left(-\gamma B^\mathsf{T} P\bar{A}x + Dv\right) \right]^\mathsf{T} P\left[B\left(-\gamma B^\mathsf{T} P\bar{A}x + Dv\right) \right] \\
&+ 2x^\mathsf{T} \bar{A}^\mathsf{T} PB\left(-\gamma B^\mathsf{T} P\bar{A}x + Dv\right).
\end{aligned}
\tag{21}
$$

For the first term of the previous equation, Rayleigh's inequality can be applied, which states that:

$$\lambda_{min}(M) x^2 \le x^\mathsf{T} M x \le \lambda_{max}(M) x^2,$$

and is applicable for any real symmetric matrix. Therefore

$$-x^\mathsf{T} Q x \le -\lambda_{min}(Q) x^2.$$

Now, for the second term of (21), it has

$$
\begin{aligned}
&\left[B\left(-\gamma B^\mathsf{T} P\bar{A}x + Dv\right) \right]^\mathsf{T} P\left[B\left(-\gamma B^\mathsf{T} P\bar{A}x + Dv\right) \right] \\
&\le \lambda_{max}\left(B^\mathsf{T} PB\right) - \gamma B^\mathsf{T} P\bar{A}x + Dv^2 \\
&\le \lambda_{max}\left(B^\mathsf{T} PB\right)\left[\begin{array}{c} \left(\gamma B^\mathsf{T} P\bar{A}x\right)^2 \\ +\gamma_1^2 D^2 x^2 + 2\gamma\gamma_1 B^\mathsf{T} P\bar{A}Dx^2 \end{array} \right] \\
&:= \eta_2(\gamma) x^2,
\end{aligned}
$$

where

$$\eta_2(\gamma) := \lambda_{max}\left(B^\mathsf{T} PB\right)\left[\gamma B^\mathsf{T} P\bar{A} + \gamma_1 D \right]^2$$

This reveals the negative contribution of the control law (18) on ΔV, allowing to define the asymptotic stability of the system (16). Analyzing the last term on the right side of the equation (21) for the equation (18), it turns out that:

$$
\begin{aligned}
2x^\mathsf{T} \bar{A}^\mathsf{T} PB\left(-\gamma B^\mathsf{T} P\bar{A}x + Dv\right) &= -2\gamma x^\mathsf{T} \bar{A}^\mathsf{T} PBB^\mathsf{T} P\bar{A}x \\
&+ 2x^\mathsf{T} \bar{A}^\mathsf{T} PBDv \\
&\le -2\gamma B^\mathsf{T} P\bar{A}^2 x^2 + 2\gamma_1 B^\mathsf{T} P\bar{A}Dx^2
\end{aligned}
$$

proposing the variables $\rho_1 = B^\mathsf{T} P\bar{A}x$ and $\rho_2 = \gamma_1 Dx$, the previous equation is rewritten as:

$$-2\gamma\rho_1^2 + 2\rho_1\rho_2 = 2\gamma\left[-\rho_1^2 + \frac{2\rho_1\rho_2}{2\gamma} \right],$$

Now, the variables $\Lambda = \dfrac{\rho_2}{2\gamma}$ and $\Pi = \rho_1$ are defined and it is known that $0 \le (\Lambda - \Pi)^2 = \Lambda^2 - 2\Pi\Lambda + \Pi^2$, then:

$$0 \leq \Lambda^2 - 2\Pi\Lambda + \Pi^2,$$

$$2\Pi\Lambda - \Pi^2 \leq \Lambda^2$$

and substituting the values of Λ and Π is obtained

$$2\gamma\left[2\frac{\rho_1\rho_2}{2\gamma} - \rho_1^2 \leq \left(\frac{\rho_2}{2\gamma}\right)^2\right],$$

$$2\gamma\left[-\rho_1^2 + 2\frac{\rho_1\rho_2}{2\gamma}\right] \leq \frac{\gamma\rho_2^2}{2\gamma^2},$$

$$-2\gamma\rho_1^2 + 2\rho_1\rho_2 \leq \frac{\rho_2^2}{2\gamma}$$

and substituting the values of ρ_1 and ρ_2 in the previous equation, it is rewritten as

$$-2\gamma B^\mathsf{T} P\bar{A}x^2 x^2 + 2\gamma_1 B^\mathsf{T} P\bar{A}Dx^2 \leq \frac{\gamma_1^2 D^2 x^2}{2\gamma}$$

$$\frac{\gamma_1^2 D^2 x^2}{2\gamma} := \delta_2(\gamma)x^2$$

where:

$$\delta_2(\gamma) := \frac{\gamma_1^2 D^2}{2\gamma},$$

the above, we have:

$$\Delta V \leq -\left(\lambda_{\min}(Q) - \eta_2 - \delta_2\right)x^2,$$

$$\lambda_{min}(Q) - \eta_2 - \delta_2 = \lambda_{min}(Q)$$

$$-\lambda_{\max}\left(B^\mathsf{T}PB\right)\left[\gamma B^\mathsf{T}P\bar{A} + \gamma_1 D\right]^2 - \frac{\gamma_1^2 D^2}{2\gamma} > 0$$

then

$$2\gamma\lambda_{min}(Q) > 2\gamma\lambda_{max}\left(B^\mathsf{T}PB\right)\left[\gamma B^\mathsf{T}P\bar{A} + \gamma_1 D\right]^2]$$

$$+\gamma_1^2 |D|^2.$$

This demonstrates that ΔV is defined negatively in a region outside a sphere centered at the origin. That is, the asymptotic stability of the system (16) under the control action (18) is concluded. □

The term $Kx(k)$ in the control law (18), which is applied to stabilize the nominal system, is obtained by means of a linear quadratic regulator and in this case, it minimizes a performance index J, given by:

$$J = \sum_{k=1}^{\infty}\left(x^\mathsf{T}(k)Qx + u^\mathsf{T}(k)Ru(k)\right)$$

(22)

where the Q and R matrices with appropriate dimensions are used to penalize the state's convergence speed and energy consumption respectively, mentioned by Kirk, D. E.[14] and Athans, M.[6].

The following section presents the experimental results, the conditions, and circumstances under which the flight is performed with the control action (18).

4 Experimental Platform

The dynamics of the hexacopter has a movement of 6 degrees of freedom (DOF), three for angular orientation and three for position. The experimental platform used allows angular movement in roll, pitch, and yaw angles (θ, ϕ and ψ) and displacements along the x, y, z axes. The coordinated control of the six rotors $\left(f1+f3+f6\right)-\left(f2+f4+f5\right)$ increase the desired z altitude, x motion is produced by changing $\left(f1+f4+f5\right)-\left(f2+f3+f6\right)$ and y motion is produced by changing $\left(f2+f5\right)-\left(f4+f6\right)$.

The platform used for testing was built on the generic "S550" airframe, made of carbon fiber and featuring a 535mm wheelbase. A "Pixhawk 2.4.8" flight controller was mounted on this chassis, which is based on a 32-bit ARM Cortex M4 core with an FPU processor running at 168MHz, 256KB of RAM, and 2MB of flash memory. The flight controller includes an integrated inertial unit, which consists of two accelerometers, two 14-bit resolution magnetometers, a 16-bit gyroscope, and an MS5611-01ba barometer with 10cm resolution. This flight controller has five UART serial ports, three receiver inputs (RF, Spektrum DSM, Futaba S.BUS, and PPM Sum Signal), an I2C port, SPI, two CAN ports, and two ADC ports. The data obtained through telemetry and GPS during the experiments were stored in a micro-SD memory card on the Pixhawk, and later processed through a program developed in MATLAB, which allows for the creation of various graphs. Furthermore, it is comprised of the following components, which can be seen in Figure 2:
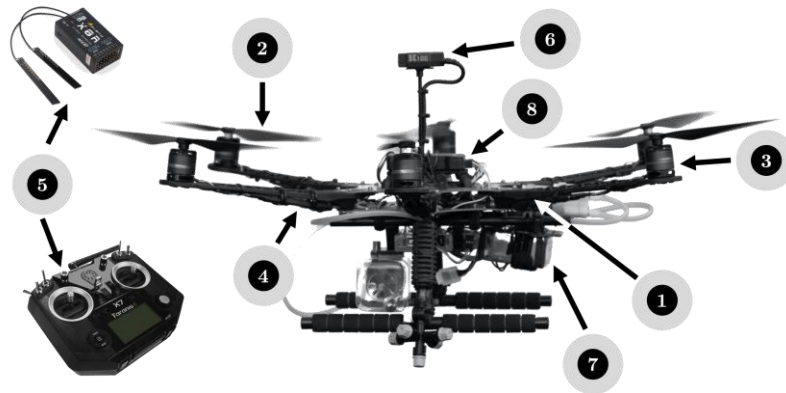
Figure 2. Elements of the hexacopter-type experimental platform.

1. Generic airframe model S550.
2. 10×4.5 inch propellers, made of polymer.
3. Brushless motors brand T-Motor of 880kV, with 435 g of thrust at 50% acceleration.
4. 40A ESC, opto type
5. 16-channel 2.4GHz FrSky Taranis X7Q transmitter, with X8R receiver in s-bus mode.
6. M8N *SE100* RadioLink GPS Module
7. LiPo batteries of 14.8v to 1550mAh, and 100c, connected in parallel.
8. Pixhawk 2.4.8 Flight Controller, with FMU V2.

The net mass of hexacopter is 1.7118 kg, which includes the elements presented in the previous list, except the transmitter.

The custom firmware that includes the programming of both the rotational and translational dynamics, together with the control law (18), was programmed in the Windows 10 Professional environment, on the IDE Eclipse Juno Release for C/C++ with the

PX4 toolchain and loaded via micro-USB on Pixhawk $2.4.8$ with Mission Planner $1.3.77$. Likewise, the calibration of the GPS, magnetometer, accelerometer, electronic speed controllers, and the binding of transmitter with receiver and calibration of channels on transmitter, was done with Mission Planner $1.3.77$.

By programming custom firmware in C++ language on the Eclipse Juno IDE for the control law (18) that includes the dynamics of rotation and translation of the hexacopter, it is possible to store signals in the micro-SD memory of the Pixhawk. These signals include current, torque, voltage, and speed in the rotors, which are determined with the help of the ESCs, as well as the x, y, and z positions and angles of roll, pitch, and yaw, which are determined by the magnetometer, gyroscope, and GPS. This allows for the state variables x_1, x_2,..., x_{12} to be obtained and their respective error variables to be generated by subtracting the actual state from the desired state, which is determined by the parametric equations of the path to follow. The error variable is then used to calculate the control signals, which are converted into voltages for the hexacopter rotors using dynamic rotation and translation equations. The voltages calculated by the FC are sent to its outputs, which are connected to the different ESCs. On one end, the ESCs are connected to the battery through the battery eliminator circuit (BEC), and on the other end, they are connected to the rotors. The voltage demanded by the ESC, together with the signal from the FC, is translated into high-frequency pulses and transmitted to the rotors through the output of each ESC, causing the rotors to turn at different speeds, which corrects their trajectory and closes the control loop. This can be seen in the schematic of Figure 3.
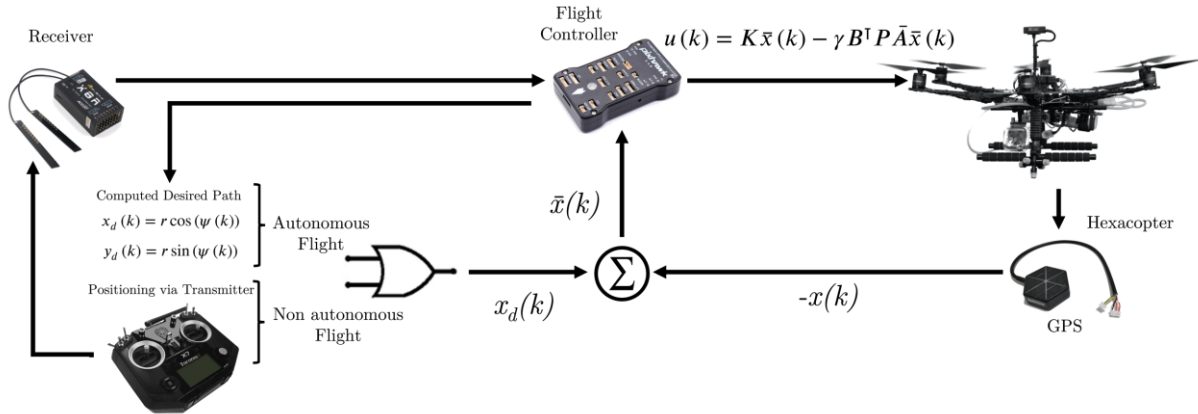
Figure 3. Scheme of Closed-loop UAV hexacopter type and control system.

It is worth mentioning that the maximum wind speed during the flight of the UAV, presented in Section 5, was measured using a XRCLIF-818 Portable Digital Anemometer. This anemometer has a range of 0 - 30m/s, a resolution of 0.1m/s, a threshold of 0.1m/s, and an accuracy of $\pm\ 5\%$.

5 Experimental Results

This section presents the numerical and experimental results that validate the control law (18) described in Section 3 and its application to the dynamics of a hexacopter-type UAV for trajectory tracking. Initially, the numerical results obtained from simulations carried out in MATLAB, both on the command line and Simulink, are presented. The results presented in subsection 5.1 provide a perspective on the considerations for the implementation and evaluation of the main proposal of this work, as well as a possible overview of the experimental results. Subsection 5.2 presents the experimental results obtained from the implementation of the control law (18), which includes stabilization and trajectory tracking tasks.

5.1 Numerical results

This subsection presents the results obtained from simulating the control law (18) on the dynamics of a hexacopter using MATLAB. It is worth noting that the results of this simulation, performed on both the MATLAB and Simulink command line, consist of a set of differential equations that establish the UAV's dynamics under the control action (18). These equations are solved using the ode8 (Dormand-Price) integration algorithm, with a fixed integration step of 1×10^{-3} and shape preservation in all integration blocks, since it is a discrete system.

Initially, the characteristics of the trajectory to be carried out, the matrices Q and R that penalize the control (18) for each subsystem in the hexacopter and the initial conditions for numerical validation are established. Subsequently, the graphic response of position, control and position error for each subsystem is presented, along with the trajectory tracking $x(k)$, $y(k)$, $z(k)$ and the description of each graph observed.

For the numerical validation, a trajectory tracking task is proposed, where the sampling time is considered equal to that of the Pixhawk, $h = 10$ ms, with the initial conditions $x(0) = 0.0$ m, $y(0) = 0.0$ m, $z(0) = 3.0$ m, $\psi(0) = 0.0^o$. The desired trajectory is defined by the parametric equations of a circumference of radius $r = 4$ m, in the form:

$$x_d(k) = r\cos(\alpha(k))$$
$$y_d(k) = r\sin(\alpha(k))$$

and $z_d(h_f) = 3.0$ m, where $\alpha(k) = 5.1566^o$ is the angle of advance every instant h in the tracking of the trajectory, which allows completing the circumference in a time of 69.8131 seconds.

The control (18) for the subsystem z is written as

$$u(k) = K_z x_z(k) - \gamma_z B_z^\mathsf{T} P_z \overline{A}_z x_z(k),$$

where the matrices $Q_z = diag(57.31, 16.35)$ and $R_z = 0.1413$ that minimize a performance index of the form (22) and $\gamma_z = 1.29512$ strengthens the control against external disturbances.

The numerical response of $z(k)$, the control action (18) and the position error in $z(k)$, with the penalty of the mentioned matrices, is observed in Figure 4.
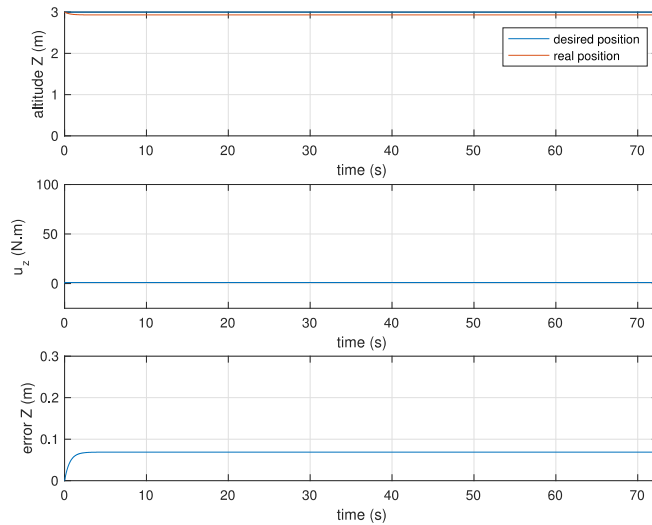
Figure 4. Altitude, error, and control signal at $z(k)$.

For the subsystem $\psi(k)$, the control law (18) is written as:

$$u_4(k) = K_\psi x_\psi(k) - \gamma_\psi B_\psi^\mathsf{T} P_\psi \bar{A}_\psi x_\psi(k)$$

where the matrices $Q_\psi = diag(29.31, 68.65)$ and $R_\psi = 1.0314$ minimize a performance index of the form (22) and $\gamma_\psi = 11.93$ robustly penalizes the control.

For $x(k) - \theta(k)$, the control action (18) is:

$$u_2(k) = K_\theta x_\theta(k) - \gamma_\theta B_\theta^\mathsf{T} P_\theta \bar{A}_\theta x_\theta(k)$$

where $Q_\theta = diag(1.41, 1.56, 1.41, 1.22)$, $R_\theta = 0.792$ minimize a performance index of the form (22) and $\gamma_\theta = 2.79$ gives robustness to the control.
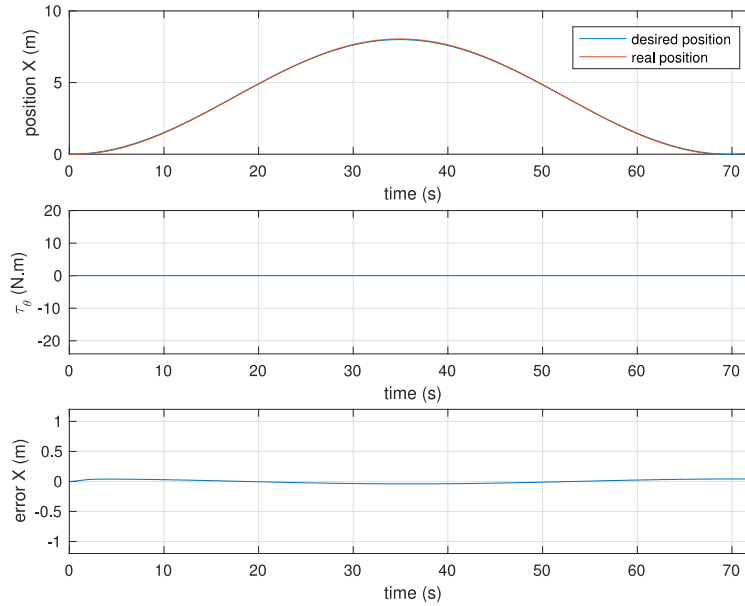
Figure 5. Position, error, and control signal at $x(k)$.

The response of $x(k)$, the control action and the error in $x(k)$, is presented in Figure 5.

For the subsystem $y(k) - \phi(k)$, the control (18) has the form:

$$u_3(k) = K_\phi x_\phi(k) - \gamma_\phi B_\phi^\mathsf{T} P_\phi \bar{A}_\phi x_\phi(k),$$

with design parameters $Q_\phi = diag(1.43, 1.15, 1.23, 0.82)$, $R_\phi = 0.82$ and $\gamma_\phi = 4.321$, which define the response of the subsystem $y(k) - \phi(k)$ shown in Figure 6.
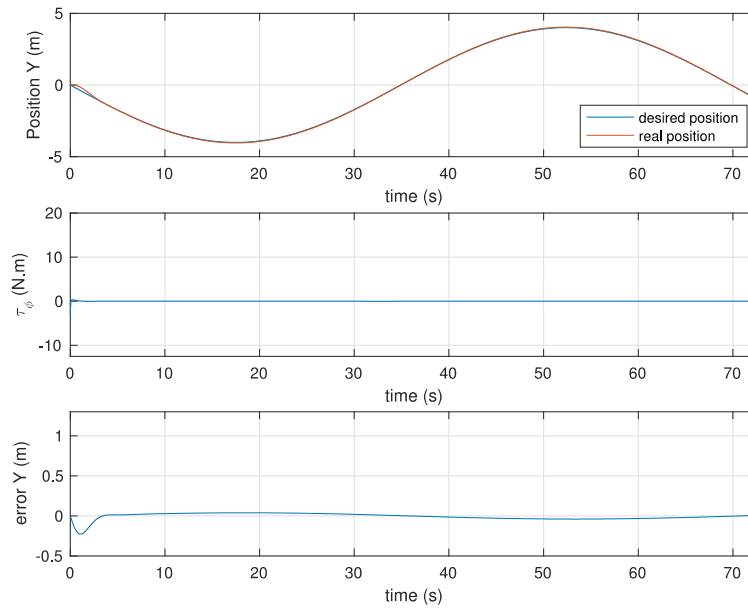
Figure 6. Position, error, and control signal at $y(k)$.

Finally, in Figure 7, the trajectory $x(k)$, $y(k)$, of the UAV is presented in the follow-up task.
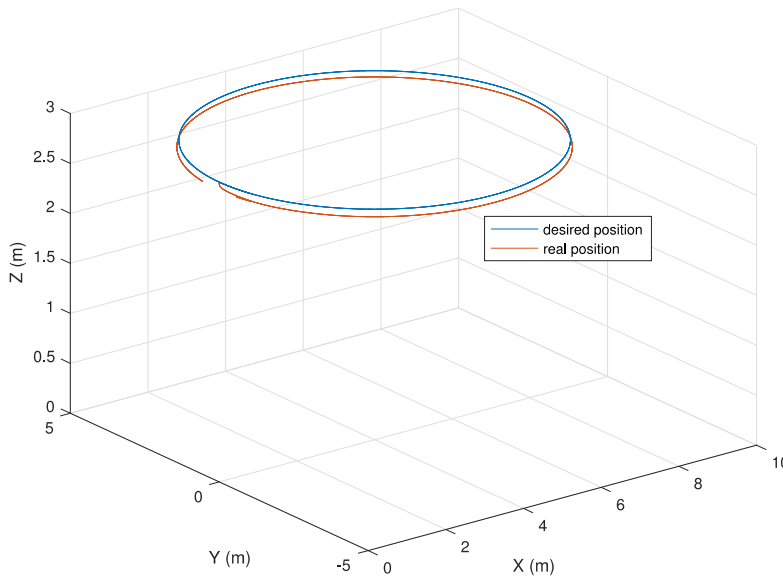
Figure 7. Trajectory tracking $x(k)$, $y(k)$, $z(k)$. $z(k)$.

The steady-state error observed in the previous graphs is mainly due to the nature of the control. In its simplest form, it is a PD controller. This error also depends on the state and control penalty in equation (18), in the design parameters Q, R, and γ. To reduce this error, an integral term can be included in its structure, which modifies the stability analysis presented in section 3. In Figures 5 and 6, smaller magnitude errors are observed than those shown in Figure 4 The reason for this behavior is associated

with the fact that the height control in Figure 4 represents a regulation task, where the reference does not change with time, and the steady-state error is evident. This is a defect of the linear nature and the PD form of the control law. In contrast, for x and y, where the reference is a function of time, the error can be reduced along the trajectory.

5.2 Experimental Results

The experimental results presented in this document were carried out in an outdoor environment with the purpose of testing the control law (18) under uncertainties that present real magnitudes, which can change in an unpredictable way over time. The task assigned to this set of experiments was to track a circular trajectory, which was chosen because the parametric equations of this trajectory allow for intense interaction between the rotational and translational dynamics of the hexacopter.

For the experiments presented graphically in this section, a sampling time $h=10ms$ is considered, with the following initial conditions: $x(0)=0.0$ m, $y(0)=0.0$ m, $z(0)=3.0$ m, $\psi(0)=0.0°$. With a maximum wind speed measured during the experiment of $5.9m/s$. And a desired trajectory that is defined by the parametric equations of the circumference, of radius $r=4m$, as:

$$x_d(k) = r\cos(\alpha(k))$$
$$y_d(k) = r\sin(\alpha(k))$$

and $z_d(hk_f) = 3.0$ m. Where $\alpha(k) = 5.1566^o$ is the angle in degrees that the trajectory advances each instant h, which defines the task execution time in 69.8131 seconds.

The control (18) for the subsystem z is written as:

$$u(k) = K_z x_z(k) - \gamma_z B_z^\mathsf{T} P_z \overline{A}_z x_z(k),$$

Where $R_z = 0.1413$, $\gamma_z = 38.9$.

For the subsystem $\psi(k)$, the control law (18) is defined as:

$$u_4(k) = K_\psi x_\psi(k) - \gamma_\psi B_\psi^\mathsf{T} P_\psi \overline{A}_\psi x_\psi(k)$$

$$Q_\psi = \begin{bmatrix} 29.31 & 0 \\ 0 & 68.65 \end{bmatrix}$$

$R_\psi = 1.0314$ y $\gamma_\psi = 11.93$.

For from $x(k) - \theta(k)$, the control action (18) is:

$$u_2(k) = K_\theta x_\theta(k) - \gamma_\theta B_\theta^\mathsf{T} P_\theta \overline{A}_\theta x_\theta(k)$$

$$Q_\theta = \begin{bmatrix} 1.41 & 0 & 0 & 0 \\ 0 & 1.56 & 0 & 0 \\ 0 & 0 & 1.41 & 0 \\ 0 & 0 & 0 & 1.22 \end{bmatrix},$$

$R_\theta = 0.792$ y $\gamma_\theta = 2.79$.

For the subsystem $y(k) - \phi(k)$, the control (18) has the form:

$$u_3(k) = K_\phi x_\phi(k) - \gamma_\phi B_\theta^\top P_\phi \bar{A}_\theta x_\phi(k),$$

$$Q_\phi = \begin{bmatrix} 1.43 & 0 & 0 & 0 \\ 0 & 1.15 & 0 & 0 \\ 0 & 0 & 1.23 & 0 \\ 0 & 0 & 0 & 0.82 \end{bmatrix},$$

$R_\phi = 0.82$ and $\gamma_\phi = 4.321$.

Figures 8, 9 and 10 are divided into three subfigures, the first one is related to position, the second one represents the control signal, and the third one shows the error signal.

Figure 8 shows the position z in the upper part, also defined as height, in which a tracking that is maintained in a region close to the reference is observed. The low magnitude oscillations are mainly due to the environmental conditions associated with wind currents.
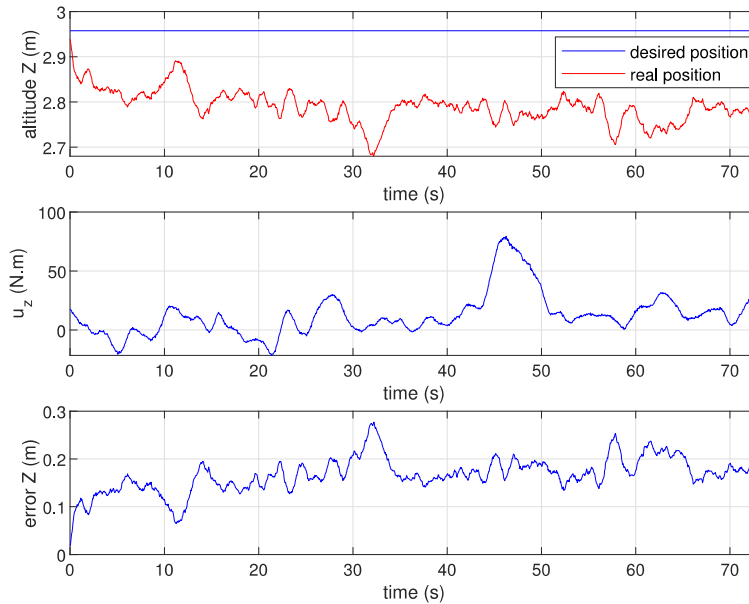
Figure 8. Altitude, error, and control signal at $z(k)$.

In Figure 9 shows the displacement in *x*, where a tracking that is maintained around the reference is observed. This figure shows that about 40 seconds after starting the tracking, the air currents manage to remove the hexacopter from the reference in position *x*.
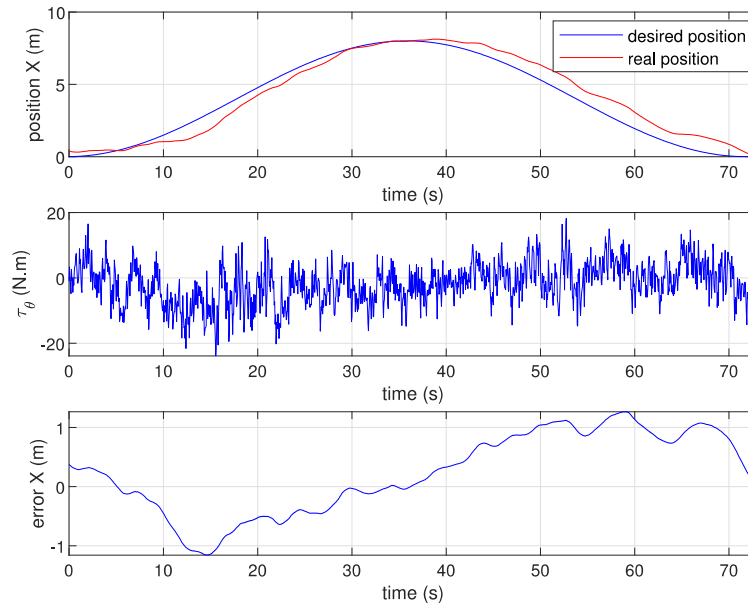
Figure 9. Position, error, and control signal at $x(k)$.

Figure 10 shows the displacement in *y*, in which a follow-up is observed that remains in a region close to the reference during 40 seconds. And the error changes over time due to the air currents that the UAV receives in different fronts.
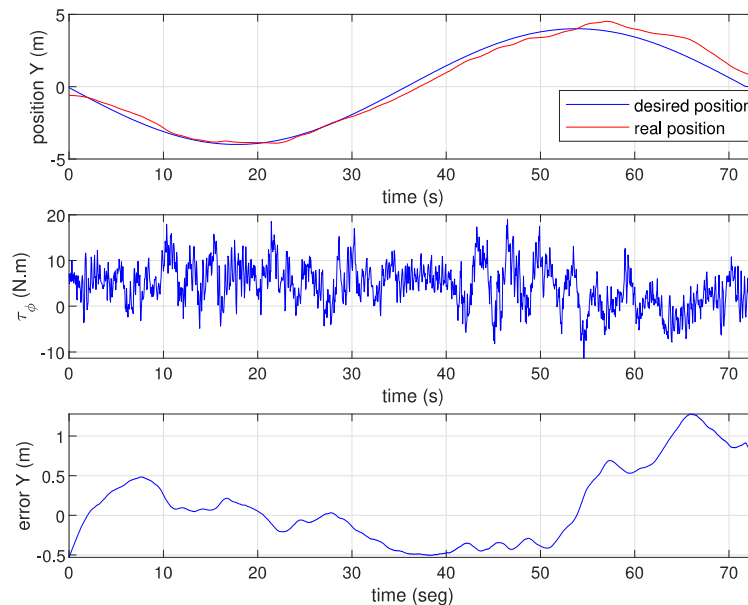
Figure 10. Position, error, and control signal at $y(k)$.

Figure 11 shows the tracking x, y, z in three-dimensional space, where the effectiveness of the control (18) is observed even when wind currents from different directions are present, with maximum speeds measured in the experiment of 5.9 m/s
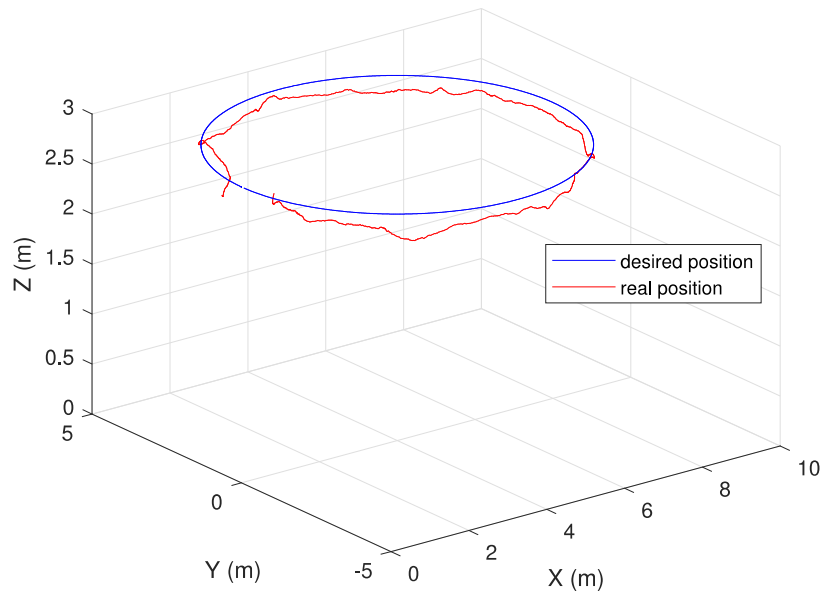
Figure 11. Trajectory tracking $x(k), y(k), z(k)$.

6   Conclusion

This paper presented experimental results of a robust discrete-time control scheme for performing hexacopter trajectory tracking tasks. It is worth noting that the performance index (22) is associated with both terms of the control law (18). The first term corresponds to a linear quadratic regulator (LQR), which is optimal in a local sense for each subsystem. The solution to the Riccati-type difference equation yields the matrix weight.

The second term provides robustness for each hexacopter subsystem. The solution of the Lyapunov equation for discrete-time linear systems improves the robustness of this control term. The   parameter in this second term allows for arbitrary modification of the robustness of each subsystem in the face of possible disturbances associated with the tasks to be performed and the flight environment. In this way, allows the possibility of establishing robustness limits to disturbances that each subsystem can be subjected to without losing stability characteristics.

References

1.   Abro, G. E. M., Bin Mohd Zulkifli, S. A., & Asirvadam, V. S. (2022). Dual-loop single-dimension fuzzy-based sliding mode control design for robust tracking of an underactuated quadrotor craft. *Asian Journal of Control*.
2.   Alaimo, A., Artale, V., Milazzo, C., Ricciardello, A., & Trefiletti, L. (2013, May). Mathematical modeling and control of a hexacopter. In *2013 International Conference on Unmanned Aircraft Systems (ICUAS)* (pp. 1043-1050). IEEE.
3.   Alaimo, A., Artale, V., Barbaraci, G., Milazzo, C. L. R., Orlando, C., & Ricciardello, A. (2016). LQR-PID control applied to hexacopter flight. *Journal of Numerical Analysis, Industrial and Applied Mathematics, 9*(3-4), 47-56.
4.   Arellano-Muro, C. A., Luque-Vega, L. F., Castillo-Toledo, B., & Loukianov, A. G. (2013, September). Backstepping control with sliding mode estimation for a hexacopter. In *2013 10th International Conference on Electrical Engineering, Computing Science and Automatic Control (CCE)* (pp. 31-36). IEEE.
5.   Artale, V., Collotta, M., Pau, G., & Ricciardello, A. (2013, October). Hexacopter trajectory control using a neural network. In *AIP Conference Proceedings* (Vol. 1558, No. 1, pp. 1216-1219). American Institute of Physics.
6.   Athans, M., & Falb, P. L. (2013). *Optimal control: An introduction to the theory and its applications*. Courier Corporation.
7.   Bai, A., Luo, Y., Zhang, H., & Li, Z. (2021). Gain robust trajectory tracking control for quadrotor UAV with unknown disturbance. *Asian Journal of Control*.
8.   Busarakum, S., & Srichatrapimuk, V. (2014, December). The design of sliding mode control of a hexarotor. In *2014 IEEE Conference on Systems, Process and Control (ICSPC 2014)* (pp. 47-52). IEEE.

9. Chen, Y. H. (1999). Optimal compensation by linear robust control for uncertain systems. *Dynamics and Control, 9*(2), 135-148.

10. Durham, W. C. (1993). Constrained control allocation. *Journal of Guidance, Control, and Dynamics, 16*(4), 717-725.

11. Falconi, G. P., & Holzapfel, F. (2016, July). Adaptive fault tolerant control allocation for a hexacopter system. In *2016 American Control Conference (ACC)* (pp. 6760-6766). IEEE.

12. García, O., Santos, O., Romero, H., & Salazar, S. (2015, November). On the tracking trajectory using optimal control in a quadrotor helicopter: Experimental results. In *2015 Workshop on Research, Education and Development of Unmanned Aerial Systems (RED-UAS)* (pp. 142-151). IEEE.

13. GrabCad Community. (2019). *DJI flamewheel F550 hexacopter frame*. https://grabcad.com/library/dji-flamewheel-f550-hexacopter-frame-1

14. Kirk, D. E. (2004). *Optimal control theory: An introduction*. Courier Corporation.

15. Khalil, H. K. (2002). *Nonlinear systems*. Upper Saddle River.

16. Lv, C., Yu, H., Zhao, N., Chi, J., Liu, H., & Li, L. (2022). Robust state-error port-controlled Hamiltonian trajectory tracking control for unmanned surface vehicle with disturbance uncertainties. *Asian Journal of Control, 24*(1), 320-332.

17. Mahmoodabadi, M. J., & Babak, N. R. (2021). Pareto optimum design of an adaptive robust backstepping controller for an unmanned aerial vehicle. *Asian Journal of Control*.

18. Moussid, M., Sayouti, A., & Medromi, H. (2015). Dynamic modeling and control of a hexarotor using linear and nonlinear methods. *International Journal of Applied Information Systems, 9*(5), 9-17.

19. Neunert, M., De Crousaz, C., Furrer, F., Kamel, M., Farshidian, F., Siegwart, R., & Buchli, J. (2016, May). Fast nonlinear model predictive control for unified trajectory optimization and tracking. In *2016 IEEE International Conference on Robotics and Automation (ICRA)* (pp. 1398-1404). IEEE.

20. Pose, C. D., Giribet, J. I., & Ghersin, A. S. (2017, June). Hexacopter fault tolerant actuator allocation analysis for optimal thrust. In *2017 International Conference on Unmanned Aircraft Systems (ICUAS)* (pp. 663-671). IEEE.

21. Rajappa, S., Ryll, M., Bülthoff, H. H., & Franchi, A. (2015, May). Modeling, control and design optimization for a fully-actuated hexarotor aerial vehicle with tilted propellers. In *2015 IEEE International Conference on Robotics and Automation (ICRA)* (pp. 4006-4013). IEEE.

22. Sanca, A. S., Alsina, P. J., & Jés de Jesus, F. C. (2010, October). Dynamic modeling with nonlinear inputs and backstepping control for a hexarotor micro-aerial vehicle. In *2010 Latin American Robotics Symposium and Intelligent Robotics Meeting* (pp. 36-42). IEEE.

23. Shao, P., Wu, J., Wu, C., & Ma, S. (2019). Model and robust gain-scheduled PID control of a bio-inspired morphing UAV based on LPV method. *Asian Journal of Control, 21*(4), 1681-1705.

24. Tripolitsiotis, A., Prokas, N., Kyritsis, S., Dollas, A., Papaefstathiou, I., & Partsinevelos, P. (2017). Dronesourcing: A modular, expandable multi-sensor UAV platform for combined, real-time environmental monitoring. *International Journal of Remote Sensing, 38*(8-10), 2757-2770.

25. Tyokumbur, E. T. (2015). Review of potential ecological impacts of peaceful robotic drone use and policy implications for developing countries. *American Journal of Environment Policy and Management, 4*, 67-71.